Polymer Chemistry

PAPER

View Article Online
View Journal | View Issue



Cite this: *Polym. Chem.*, 2017, **8**, 5228

# Introduction of anti-fouling coatings at the surface of supramolecular elastomeric materials *via* post-modification of reactive supramolecular additives†

Olga J. G. M. Goor,[a,b] Joyce E. P. Brouns[a,b] and Patricia Y. W. Dankers *[a,b]

Protein repellent coatings have been extensively studied to introduce anti-fouling properties at material surfaces. Here we introduce a covalent anti-fouling coating at the surface of supramolecular ureidopyrimidinone (UPy) based materials introduced *via* post-modification of reactive UPy-functionalized tetrazine additives incorporated into the supramolecular polymer material. After material formulation, an anti-fouling coating comprised of bicyclononyne (BCN) functionalized poly(ethylene glycol) (PEG) polymers was reacted. This coating was covalently attached to the surface *via* a highly selective electron-demand Diels–Alder cycloaddition between tetrazine and BCN. The anti-fouling properties of three different BCN-PEG polymers, mono-functional-PEG-BCN, bi-functional-PEG-BCN and star-PEG-BCN, respectively, were systematically studied. The mono-functional-PEG-BCN showed minor reduction in both protein adsorption and cell adhesion, whereas the bi-functional-PEG-BCN and the star-PEG-BCN polymer coating demonstrated complete anti-fouling performance, both towards protein adhesion as well as cell adhesion. Additionally, a bioorthogonal ligation strategy was performed in culture medium in the presence of cells showing a similar behavior for the three anti-fouling coatings, which indicates that this strategy can be applied for post-modification reactions in a complex environment.

Received 13th May 2017,
Accepted 19th June 2017

DOI: 10.1039/c7py00801e

rsc.li/polymers



## Introduction

Surface interactions play an important role upon implantation of a biomaterial, as the surface of the material is the first to interact with the *in vivo* environment.[1] Therefore, control on surface composition and activity are important factors in the design of biomaterials. Surface modifications to introduce surface functionality can be achieved following a broad scope of different strategies, *i.e.* physical adsorption, covalent modification and incorporation of biomimetic cues.[2] However, biofouling of the material surface is of great concern due to its impact on the availability of activity and functionality as a result of nonspecific protein adsorption.[3]

Upon implantation of a biomaterial, a tissue response is initiated with the non-specific adsorption of proteins at the material surface,[4] which could ultimately lead to biomaterial failure.[5] High mobility proteins, such as albumin, are the first to adsorb. Subsequently, displacement by less abundant proteins with higher affinity occurs, starting with globulin and fibrinogen, which are then later replaced by high molecular weight kininogen. This process is called the Vroman effect.[6]

The inhibition of protein adsorption is therefore critical in order to prevent biomaterial failure.[7,8] To this end, hydrophilic and zwitterionic polymers are widely applied in the design of anti-fouling materials, to allow the formation of a hydration layer at the surface which in turn prevents adsorption onto the surface.[9] Surface functionalization strategies based on the use of poly(ethylene glycol) (PEG) polymers are extensively studied to impart adhesion resistance.[10–14] Among these are self-assembling monolayers (SAMs),[5,12,15] polymer brushes based on PEG and zwitterionic moieties immobilized on different substrates[16–20] and the covalent introduction of PEG polymers based on click chemistry.[21,22] Moreover, PEG polymers can be anchored at different materials and substrates *via* the introduction of triblock copolymers,[23–25] in a supramolecular fashion by the post-modification of polymeric membranes based on cyclodextrin host–guest chemistry[26] or introduced at the surface of electrospun polyurethane (PU) fibers.[27] Additionally, multi-armed PEG polymers can be introduced at substrate surfaces to yield anti-fouling behavior.[28,29] Another

[a]*Institute for Complex Molecular Systems, Eindhoven University of Technology, P.O. Box 513, 5600 MB Eindhoven, The Netherlands. E-mail: p.y.w.dankers@tue.nl*
[b]*Laboratory of Chemical Biology, Department of Biomedical Engineering, P.O. Box 513, 5600 MB Eindhoven, The Netherlands*

†Electronic supplementary information (ESI) available. See DOI: 10.1039/c7py00801e

elegant approach is the anchoring of PEG polymers at surfaces *via* dopamine or catechol moieties.[30,31]

In our group, we developed supramolecular biomaterials based on the quadruple hydrogen bonding ureidopyrimidinone (UPy) motif that yields supramolecular thermoplastic elastomer materials upon pre-polymer end-functionalization.[32,33] *Via* a modular approach, bioactive cues equipped with a UPy-moiety can be incorporated into these materials giving rise to a platform of material functionalization.[34,35] The incorporation of anti-fouling UPy-based polymers and additives have previously been reported in the development of functional biomaterials.[36,37] Moreover, anti-fouling biomaterials could be reactivated upon the incorporation of only small amounts of UPy-functionalized peptides.[38] Nevertheless, this anti-fouling behavior showed only a short-term effect both *in vitro* and *in vivo* and displayed minor protein adsorption prevention.[37] A strategy based on the covalent post-modification of the supramolecular thermoplastic elastomer surface *via* the modular incorporation of a reactive additive was more recently proposed. This approach allows for solely surface modification and yet provides a method to decouple the material processing conditions and post-functionalization.[39]

The anti-fouling coating is introduced at the surface of supramolecular materials (Fig. 1a) *via* the selective modification of a reactive UPy-modified tetrazine (UPy-Tz) additive (Fig. 1c, **2**), which is modularly incorporated in telechelically UPy-modified polycaprolactone (PCLdiUPy) (Fig. 1b, **1**), thereby providing a handle for selective surface post-modification *via*

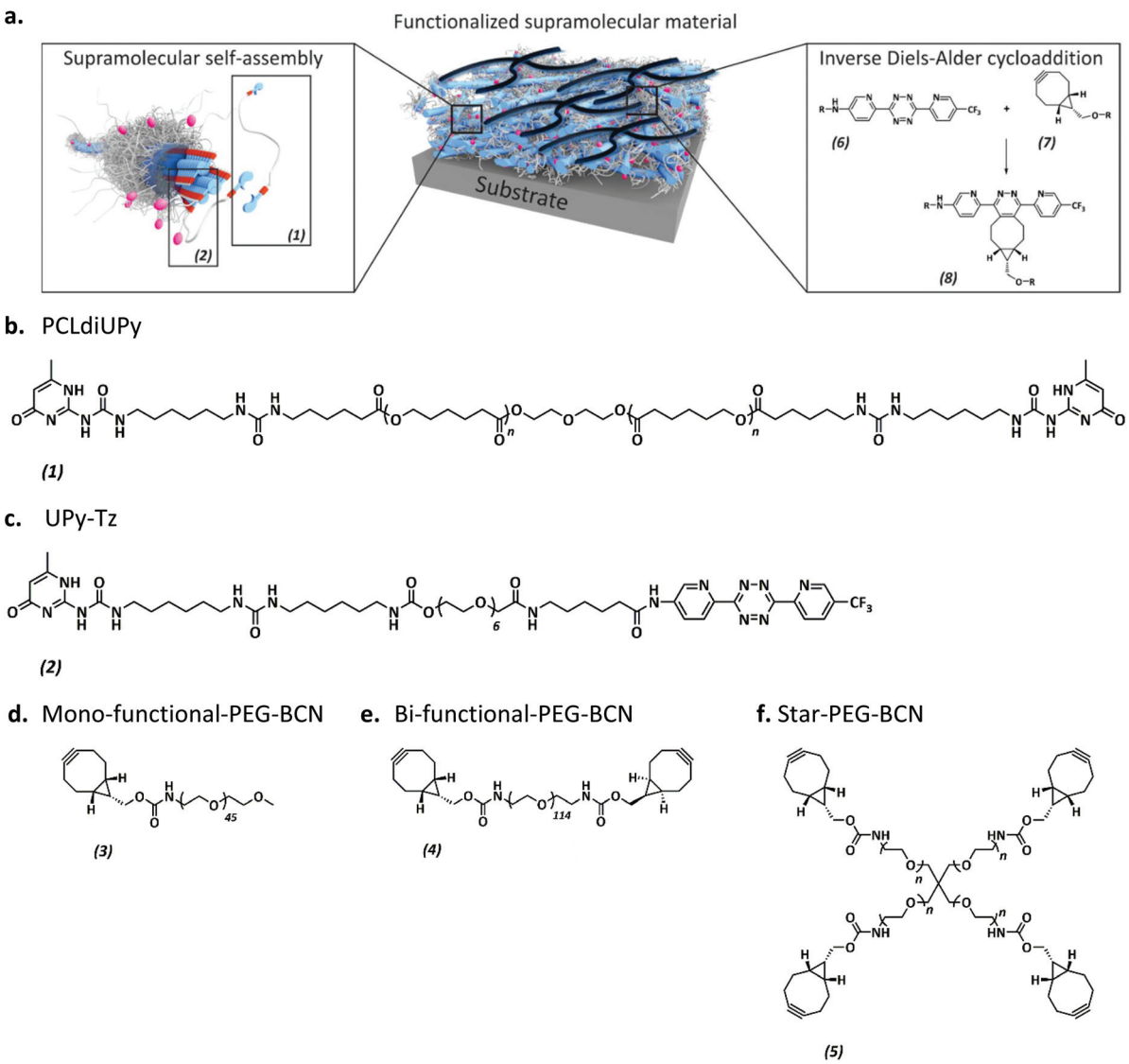


**Fig. 1** Functionalization of supramolecular materials with an anti-fouling coating, (a) schematic representation of the functionalization, with on the left the supramolecular self-assembly of the UPy-functionalized polymer (PCLdiUPy, **1**) with the UPy-additive (UPy-Tz, **2**) and the highly selective inverse Diels–Alder cycloaddition (iEDDA) on the right. Chemical structures of (b) $PCL_{2k}$diUPy (**1**), (c) UPy-Tz additive (**2**), (d) mono-functional-$PEG_{2k}$-BCN, (e) bi-functional-$PEG_{5k}$-BCN and (f) star-$PEG_{10k}$-BCN are shown.

an inverse electron demand Diels–Alder cycloaddition.[40,41] Three different poly(ethylene glycol) (PEG) polymers modified with bicyclononyne (BCN) moieties, mono-functional-$PEG_{2k}$-BCN (Fig. 1d, **3**), bi-functional-$PEG_{5k}$-BCN (Fig. 1e, **4**) and star-$PEG_{10k}$-BCN (Fig. 1f, **5**), respectively, were synthesized and introduced to facilitate the anti-fouling function. It is hypothesized that the bi-functional-PEG-BCN and star-PEG-BCN polymer coatings display excellent anti-fouling properties as a result of their ability to form cyclic loops at the material interface.[42] The mono-functional-PEG-BCN has one anchor point at the supramolecular material surface, whereas the bi-functional-PEG-BCN is in theory able to anchor both ends of the polymer onto the surface. The star-PEG-BCN not only contains four anchor points, the molecular weight of the PEG in this polymer is higher as well, while at the same time the BCN : PEG ratio is kept constant for all three conjugates. The tunability and the properties of the anti-fouling coating were assessed both by protein adsorption examination by quartz crystal microbalance with dissipation monitoring (QCM-D) as well as cell adhesion studies. Moreover, the bioorthogonal ligation strategy was performed in a complex medium, in the presence of cells.

## Results and discussion

### Material characterization

The surface morphology of the spin-coated films of PCLdiUPy, PCLdiUPy with UPy-Tz (10 mol%) before and after functionalization with star-PEG-BCN (**5**) was assessed using AFM (Fig. 2a–c). A nanofiber morphology is observed, indicating that the UPy-Tz is incorporated into the PCLdiUPy nanofibers (Fig. 2a and b). After the reaction with the star-PEG-BCN (Fig. 2c) the fibrous structures are still present, however in a less defined fashion. Moreover, introduction of the star-PEG-BCN did not change roughness of the surfaces (ESI Fig. S1†).

The surface composition of the spin-coated materials both before and after modification with an anti-fouling PEG-BCN polymer was investigated using XPS (Fig. 2d). Upon the introduction of the mono-functional-PEG-BCN (**2**) and bi-functional-PEG-BCN (**4**) polymers, the carbon content (73.5 atom% and 72.6 atom%, respectively) decreases compared to the PCLdiUPy (74.4 atom%) and the PCLdiUPy with UPy-Tz (74.0 atom%) surfaces. Concomitantly, an increase in the oxygen content is observed after the modification of the surface with the hydrophilic PEG polymers and this increase is in line with a higher molecular weight PEG and more BCN functionalities (20.5 atom% for mono-functional-PEG-BCN, 20.8 atom% for bi-functional-PEG-BCN and 22.1 atom% for star-PEG BCN, respectively). The nitrogen content of the PCLdiUPy surface with UPy-Tz increases compared to the bare PCLdiUPy surface (6.0 atom% compared to 5.5 atom%), which is explained by a nitrogen rich molecular structure of the tetrazine moiety. This result indicates that UPy-Tz is enhanced at the surface of the material.[39] A decrease in the nitrogen content is observed after the modification of the surface with bi-functional-PEG-BCN (**4**) and star-PEG-BCN (**5**) (4.8 atom% and 5.1 atom%, respectively) compared to the bare PCLdiUPy surface (5.5 atom%). An increase of fluorine to 0.2 atom% was detected after surface modification with the hydrophilic PEG polymers, which could be an effect of the incubation in aqueous medium that results from the rearrangement of UPy-Tz at the supramolecular material surface.[39]

The wettability of the modified surfaces was investigated by static water contact angle measurements. No major changes were observed for the bare PCLdiUPy surface and the PCLdiUPy surface after incubation with the mono-functional-PEG-BCN (**3**), bi-functional-PEG-BCN (**4**) and star-PEG-BCN (**5**)

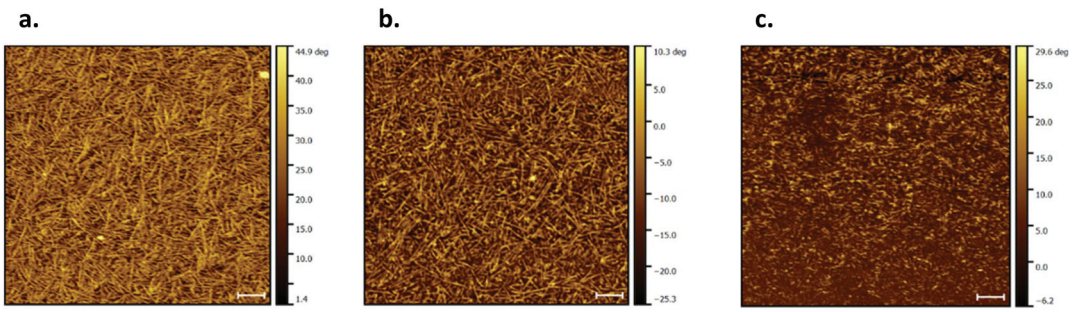


d.

| | C [%] | N [%] | O [%] | F [%] |
|---|---|---|---|---|
| PCLdiUPy | 74.4 | 5.5 | 20.1 | 0 |
| PCLdiUPy + UPy-Tz | 74.0 | 6.0 | 20.0 | 0.1 |
| PCLdiUPy + UPy-Tz + Mono-PEG | 73.5 | 5.9 | 20.5 | 0.2 |
| PCLdiUPy + UPy-Tz + Bi-PEG | 74.2 | 4.8 | 20.8 | 0.2 |
| PCLdiUPy + UPy-Tz + Star-PEG | 72.6 | 5.1 | 22.1 | 0.2 |

e.

| Surface | WCA (°) | Surface | WCA (°) |
|---|---|---|---|
| PCLdiUPy | 68.0 ± 0.50 | PCLdiUPy + UPy-Tz | 70.1 ± 0.54 |
| PCLdiUPy + Mono-PEG | 67.7 ± 0.35 | PCLdiUPy + UPy-Tz + Mono-PEG | 63.1 ± 2.50 |
| PCLdiUPy + Bi-PEG | 69.7 ± 1.20 | PCLdiUPy + UPy-Tz + Bi-PEG | 58.2 ± 0.61 |
| PCLdiUPy + Star-PEG | 66.5 ± 1.09 | PCLdiUPy + UPy-Tz + Star-PEG | 48.6 ± 1.24 |

Fig. 2 Surface characterization of the different material films with AFM, XPS and water contact angle. AFM phase micrographs of PCLdiUPy (a), PCLdiUPy with 10 mol% UPy-Tz (b) and after star-PEG-BCN functionalization (c), (d) XPS compositional table of the different surfaces and (e) water contact angles of the respective surfaces. Five measurements were performed per surface and standard deviations are plotted.

 

polymers (68.0°, 67.7°, 69.7° and 66.5°, respectively). In contrast, the PCLdiUPy with 10 mol% UPy-Tz prior to and after modification with the mono-functional-PEG-BCN (**3**), bi-functional-PEG-BCN (**4**) and star-PEG-BCN (**5**) polymers show a clear drop in contact angle values (70.1°, 63.1°, 58.2° and 48.6°, respectively) (Fig. 2e). These results indicate that the PEG-BCN polymers show minor non-specific interactions with the PCLdiUPy surfaces, whereas an increased hydrophilicity of the surfaces is observed after the modification of the PCLdiUPy with UPy-Tz surfaces. Interestingly, the hydrophilicity of the surface increases as a result of the architecture of the PEG-polymer, *i.e.* the molecular weight of the PEG polymer per BCN-moiety is kept constant (~2–2.5 kDa). The star-PEG-BCN and bifunctional-PEG-BCN are able to attach to the surface with all end groups, whereas the monofunctional-PEG-BCN has only one BCN group available, which might result in a different surface packing. Depending on the polymer architecture the surface properties of the materials can be tuned.

The direct proof of the covalent post-modification of the supramolecular surface was obtained *via* surface MALDI-ToF MS measurements, confirming the reaction product (**10**) of the UPy-Tz (**2**) reacted with a BCN-$NH_2$ (**9**) model compound was formed (ESI Fig. S2†).

In conclusion, the supramolecular surfaces show a fibrous morphology, and the UPy-Tz was successfully incorporated into the supramolecular nanofibers, thereby not changing the fiber morphology. Upon introduction of the PEG-BCN polymers, differences in the chemical composition of the surfaces were observed, indicative of effective surface modification. On a macroscopic scale, an increase in the hydrophilicity of the surfaces was measured after the introduction of the PEG-BCN polymers at the PCLdiUPy with 10 mol% UPy-Tz surfaces.

### Protein adsorption measurements

Next, the properties of the modified materials were investigated. The intrinsic fouling properties of our supramolecular materials modified with the PEG-BCN polymers were examined using QCM-D, by administering the first three proteins of the Vroman series (bovine serum albumin (BSA, 30 mg $mL^{-1}$), γ-globulin (10 mg $mL^{-1}$) and fibrinogen (3 mg $mL^{-1}$)).

First, the fouling properties towards the BSA adsorption of pristine supramolecular PCLdiUPy and the PCLdiUPy with 10 mol% UPy-Tz surfaces were studied (ESI Fig. S3†). After equilibration, the BSA is flowed for 30 minutes and subsequently the surfaces are rinsed to remove all the non-adsorbed BSA. The PCLdiUPy with UPy-Tz incorporated shows a decrease in BSA adsorption compared to the PCLdiUPy surface, which is attributed to the presence of the UPy-Tz at the material surface that is composed of a polar tetrazine moiety and a hydrophilic oligo(ethylene glycol) spacer, which might give rise to a slightly more hydrophilic supramolecular surface. Moreover, in order to optimize the extent of anti-fouling behavior upon BSA administration, various star-PEG-BCN (**5**) concentrations were conjugated at the surface of PCLdiUPy with UPy-Tz (ESI Fig. S3†). These results show the tunability of the anti-fouling behavior and modulation based on the star-PEG-BCN concentration that was applied. Therefore, 0.5 mg $mL^{-1}$ star-PEG-BCN concentration was chosen to continue experiments within this paper.

QCM-D measurements were performed to quantify the amount of proteins adsorbed onto the supramolecular surfaces under physiologically relevant conditions. The Vroman series was applied on the different surfaces, PCLdiUPy and PCLdiUPy with 10 mol% UPy-Tz, that were modified with either mono-functional-PEG-BCN (**3**), bi-functional-PEG-BCN (**4**) or star-PEG-BCN (**5**). Both the change in frequency ($\Delta f$) and dissipation ($\Delta D$) were monitored over time. After the equilibration of the signal, the protein mixture was applied (time point I) and after 30 minutes the surfaces were rinsed to remove all non-adsorbed proteins (time point II) (Fig. 3a–c). It was hypothesized that the PCLdiUPy surfaces show the largest $\Delta f$, indicative of a higher mass adsorption. The increase in the molecular mass of the PEG polymers and the additional BCN moieties that are available for the surface reaction of the mono-functional-PEG-BCN, bi-functional-PEG-BCN and star-PEG-BCN, respectively, are envisioned to increase the anti-fouling properties of the surface alongside. Upon mono-functional-PEG-BCN modification, the remaining frequency and dissipation shifts for the PCLdiUPy surface are larger than for the PCLdiUPy with UPy-Tz surfaces (−65 Hz, $5 \times 10^{-6}$ and −30 Hz and $2 \times 10^{-6}$, respectively), which indicates a reduction in mass adsorption at the surfaces that were covalently modified with mono-functional-PEG-BCN (Fig. 3a). For the bi-functional-PEG-BCN a similar trend is observed for the frequency and dissipation values of the PCLdiUPy and PCLdiUPy with UPy-Tz surfaces (−55 Hz, $4 \times 10^{-6}$ and −35 Hz and $5 \times 10^{-6}$, respectively) (Fig. 3b). The dissipation shifts at the modified surfaces are higher compared to the mono-functional-PEG-BCN functionalized surfaces. This might be explained by a different packing of the PEG-BCN polymer coating at the surfaces. The higher dissipation values at the bi-functional-PEG-BCN surfaces indicate that a more visco-elastic layer is formed. For the star-PEG-BCN functionalization (Fig. 3c), both the frequency and dissipation shifts of the PCLdiUPy surfaces are larger than the PCLdiUPy with UPy-Tz surfaces (−45 Hz, $7 \times 10^{-6}$ and −15 Hz and $2 \times 10^{-6}$, respectively), which indicates that the star-PEG-BCN coating successfully decreases protein adsorption. Since the dissipation values for all the different experiments are >5–10% of the $\Delta f$, a Voigt–Voinova visco-elastic model was applied to analyze the datasets. A summary of all the results shows the areal mass adsorption (ng $cm^{-2}$) for the different surfaces (Fig. 3d). No significant differences were observed for the PCLdiUPy surfaces that were incubated with the different PEG-BCN polymers. Upon the incorporation of 10 mol% UPy-Tz, a significant reduction in protein adsorption can be appreciated. In addition, the protein adsorption gradually decreases in the series of mono-functional-PEG-BCN (**3**), bi-functional-PEG-BCN (**4**) and star-PEG-BCN (**5**) polymers, respectively.

Mass adsorption on the PCLdiUPy with UPy-Tz surfaces modified with star-PEG-BCN for the individual proteins as well

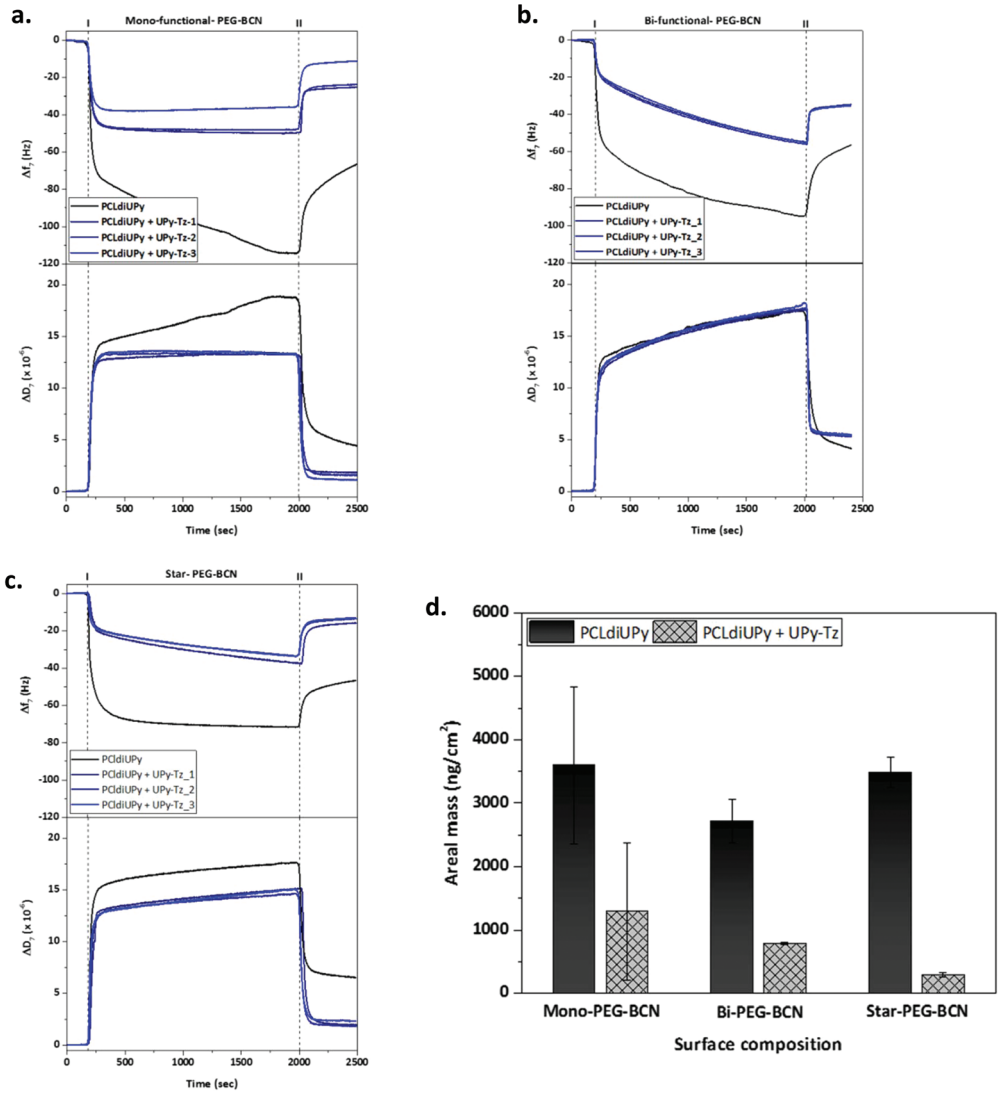


**Fig. 3** Quartz crystal microbalance with dissipation monitoring (QCM-D) results after Vroman series adsorption (30 mg $mL^{-1}$ BSA, 10 mg $mL^{-1}$ γ-Globulin and 3 mg $mL^{-1}$ fibrinogen) onto PCLdiUPy or PCLdiUPy with 10 mol% UPy-Tz ($n$ = 3, UPy-Tz_1, UPy-Tz_2 and UPy-Tz_3, respectively) surfaces, at time point I the protein mixtures were administered to the surface and at time point II the surfaces were exposed to PBS buffer, (a) frequency and dissipation responses at surfaces modified with 0.5 mg $mL^{-1}$ mono-functional-PEG-BCN, (b) frequency and dissipation responses at surfaces modified with 0.5 mg $mL^{-1}$ bi-functional-PEG-BCN, (c) frequency and dissipation responses at surfaces modified with 0.5 mg $mL^{-1}$ star-PEG-BCN and (d) corresponding graph that plots the mass adsorption (ng $cm^{-2}$) on the modified surfaces. All the data represented in the graph results from visco-elastic modeling using a Voigt–Voinova model. Averages of $n$ = 3 measurements are plotted with the corresponding standard deviations.

as the mixture is provided, which clearly shows the anti-fouling properties of the modified surfaces for the individual proteins as well as the mixture of the Vroman series (ESI Fig. S4†).

In conclusion, all three different PEG-BCN coatings were able to reduce protein adsorption at the material surface. However, star-PEG-BCN significantly outperforms the mono-functional-PEG-BCN and bi-functional-PEG-BCN polymer in its ability to prevent protein adsorption.

### Cell adhesion studies

To further investigate the surface properties of the modified supramolecular biomaterials, their ability to prevent cell adhesion was studied. A strong correlation exists between protein adsorption with both adhesion and spreading of cells. The cells recognize protein structures at the biomaterial surface and along with the surface properties of the material, the initial cell behavior on the biomaterial surface is affected.[43] The cells bind to ECM components adsorbed at the material surface through integrin receptors, which upon clustering form focal adhesions that represent a structural link between the cytoskeleton and the biomaterial surface.[44] The cell adhesion and spreading of human kidney (HK-2) cells were studied on the different supramolecular surfaces prior to and after modification with the PEG-BCN hydrophilic

 

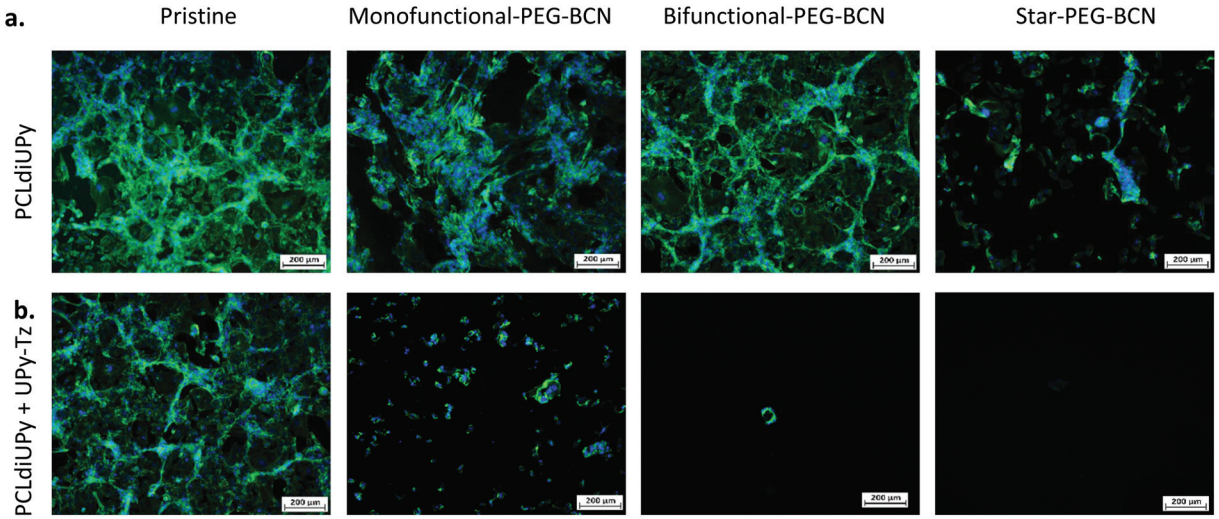


**Fig. 4** Fluorescence microscopy graphs of HK-2 cells on spin-coated surfaces after 7 days of culture. Upper row represents images of PCLdiUPy (a), the pristine material or incubated with either mono-functional-PEG-BCN, bi-functional-PEG-BCN or star-PEG-BCN (from left to right). Lower row represents images of PCLdiUPy with 10 mol% UPy-Tz incorporated (b) the pristine material or incubated with either mono-functional-PEG-BCN, bi-functional-PEG-BCN or star-PEG-BCN (from left to right). The actin skeleton is stained with phalloidin (green), the nuclei are stained with DAPI (blue). Scale bars represent 200 μm.

polymers, 24 h after seeding (ESI Fig. S5†). Moreover, the adhesion of the cells on the pristine surfaces (PCLdiUPy and PCLdiUPy with 10 mol% UPy-Tz) clearly shows the vinculin-rich focal adhesions after 72 h of culture, indicating the cells adhered on these biomaterial surfaces (ESI Fig. S6†). The PCLdiUPy and PCLdiUPy with UPy-Tz surfaces show cell attachment and spreading. The incubation of the PCLdiUPy surfaces with the mono-functional-PEG-BCN and bi-functional-PEG-BCN does not have any influence on the cell adhesion and morphology, whereas the incubation with star-PEG-BCN shows a reduction in the amount of cells adhered at the surface. The PCLdiUPy with UPy-Tz surfaces that were modified with mono-functional-PEG-BCN show only a minor reduction in cell adhesion and spreading, indicating that the mono-functional-PEG-BCN is not able to completely cover the surface and thereby prevent cell attachment. In contrast, the modification of the PCLdiUPy with UPy-Tz surfaces with bi-functional-PEG-BCN and star-PEG-BCN show a significant reduction in the amount of cells present at the surface. Additionally, the cells adapt a round morphology, indicating they were not able to adhere or spread on these surfaces. Both the bi-functional-PEG-BCN and the star-PEG-BCN were able to effectively create a cell-repellent material surface.

In order to investigate the development of these coatings in time, cell morphology and spreading were studied after 7 days of culture (Fig. 4). The pristine PCLdiUPy and PCLdiUPy with UPy-Tz surfaces show a confluent layer at the material surface. For both mono-functional-PEG-BCN and bi-functional-PEG-BCN incubation on the PCLdiUPy surfaces, the cell adhesion and morphology were not affected. However, the star-PEG-BCN incubation on the PCLdiUPy surface shows a reduction in cell adhesion, which suggests the star-PEG-BCN non-specifically interacts with the PCLdiUPy surface. In contrast to the 24 h culture period, the mono-functional-PEG-BCN functionalization of the PCLdiUPy with the UPy-Tz surface shows a reduction in cell adhesion and spreading at the surface, however no complete anti-fouling effect was observed. The bi-functional-PEG-BCN and star-PEG-BCN modified PCLdiUPy with UPy-Tz surfaces show complete prevention of cell attachment 7 days after cell seeding, demonstrating the effective introduction of an anti-fouling coating.

Another interesting examination was to address the effectiveness of the post-modification reaction in the presence of cells in a cell culture medium. To this end, the PEG-BCN polymers were diluted in a complex medium and mixed with the cells prior to administration on the PCLdiUPy and PCLdiUPy with UPy-Tz surfaces. Cell adhesion and morphology were studied 24 h (Fig. 5) after seeding. For the pristine PCLdiUPy and PCLdiUPy with UPy-Tz surfaces and the PCLdiUPy surfaces with mono-functional-PEG-BCN, bi-functional-PEG-BCN or star-PEG-BCN present in the culture medium, cell adhesion and spreading were observed despite the presence of the PEG-BCN polymers in the culture medium. On the PCLdiUPy surfaces that were incubated with the mono-functional-PEG-BCN and bi-functional-PEG-BCN in the culture medium, a near confluent layer of cells was observed. These results indicate that the presence of the hydrophilic PEG-BCN polymers did not change the adhesion and spreading properties of the cells.

The PCLdiUPy with UPy-Tz surfaces with mono-functional-PEG-BCN, bi-functional-PEG-BCN or star-PEG-BCN present in the culture medium with the cells were hypothesized to display anti-fouling properties due to the effective click

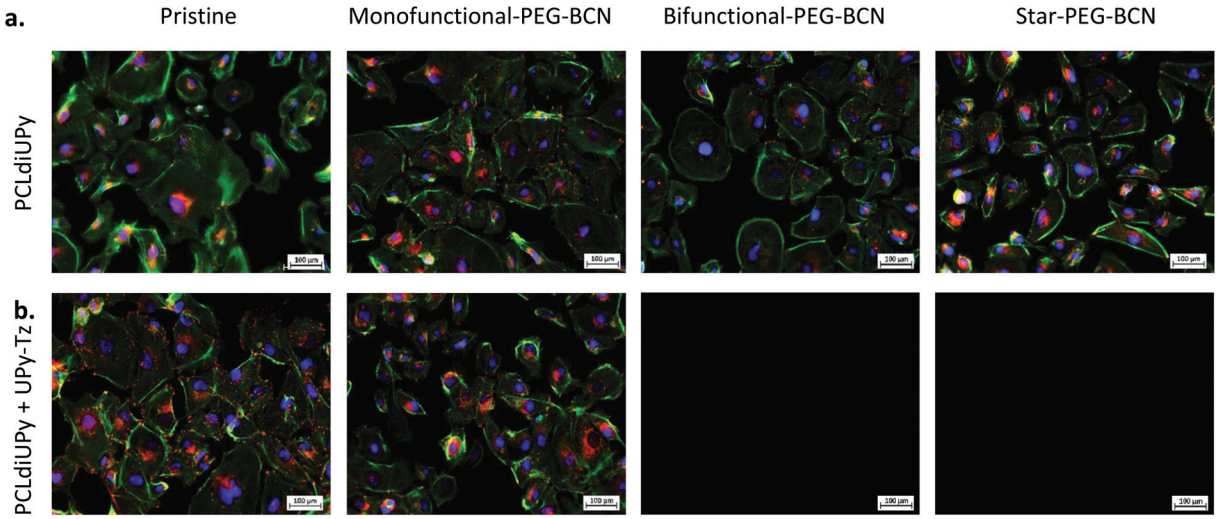


**Fig. 5** Fluorescence microscopy graphs of the cycloaddition reaction in the complex medium in the presence of HK-2 cells on spin-coated surfaces after 24 hours of culture. Upper row represents images of PCLdiUPy (a), the pristine material or incubated with either mono-functional-PEG-BCN, bi-functional-PEG-BCN or star-PEG-BCN (from left to right). Lower row represents images of PCLdiUPy with 10 mol% UPy-Tz incorporated (b) the pristine material or incubated with either mono-functional-PEG-BCN, bi-functional-PEG-BCN or star-PEG-BCN (from left to right). The actin skeleton is stained with phalloidin (green), the nuclei are stained with DAPI (blue) and the focal adhesions were stained with Atto-555 (red). Scale bars represent 100 μm.

reaction between the reactive UPy-Tz additive and the BCN-functionality on the PEG polymers, which was reported to be performed in the complex medium and living systems.[41,45–47] The PCLdiUPy with UPy-Tz surfaces incubated with mono-functional-PEG-BCN present in the culture medium with the cells, a reduction of cell attachment was observed (Fig. 5), hence the surface did not display complete anti-fouling behavior. For the PCLdiUPy with UPy-Tz surfaces that were incubated with bi-functional-PEG-BCN or star-PEG-BCN present in the culture medium with the cells, no cells were observed, indicating that the surfaces were completely anti-fouling and thereby prevent cell adhesion (Fig. 5). In conclusion, the presence of the bi-functional-PEG-BCN and the star-PEG-BCN in the culture medium with the cells could completely prevent cell adhesion at the PCLdiUPy with UPy-Tz surfaces, which demonstrate the high efficiency of the reaction between the UPy-Tz and the BCN-modified PEG polymers, even in the presence of the complex medium and cells.

# Experimental

## Methods

$^1$H-NMR data were recorded on a Bruker Cryomagnet for NMR spectroscopy (400 MHz) at room temperature. Proton experiments were reported in parts per million (ppm) downfield of TMS. The $^1$H-NMR data are reported as following: chemical shift, multiplicity (s = singlet, d = doublet, t = triplet, q = quartet, m = multiplet) and integration. Matrix-assisted laser desorption ionization time-of-flight mass spectrometry (MALDI-ToF MS) was performed on a PerSeptive Biosystems Voyager-DE PRO spectrometer using an α-cyano-4-hydroxycinnamic acid matrix.

## Materials

All reagents and solvents were purchased from Sigma Aldrich and used as received, unless stated otherwise. PCLdiUPy and UPy-Tz compounds were synthesized by SyMO-Chem BV (Eindhoven, The Netherlands).[1,11] (1*R*,8*S*,9*s*)-Bicyclo[6.1.0]non-4-yn-9-ylmethyl *N*-succinimidyl carbonate was purchased from Sigma Aldrich (Zwijndrecht, The Netherlands). Methoxide PEG-amine HCL salt and PEG diamine HCL salt were purchased from Jenkem Technology (Texas, USA). Star-PEG BCN was kindly provided by Maxime Grillaud, Eindhoven University of Technology, Eindhoven, The Netherlands. Mono-functional-PEG-BCN and bi-functional-PEG-BCN were synthesized as described. Phosphate buffered saline (PBS), 1,1,1,3,3,3-hexafluoro-2-propanol (HFIP), Triton X-100 buffer and 37 wt% formaldehyde solution were purchased from Sigma-Aldrich. Ammonia, hydrogen peroxide and sulphuric acid were obtained from VWR (Amsterdam, The Netherlands). Dulbecco's Modified Eagle Medium (DMEM), trypsin-EDTA (25300-054), heat inactivated fetal bovine serum (FBS, 26140-079) and penicillin–streptomycin solutions were obtained from Gibco (Thermo Fisher Scientific, USA). Monoclonal IgG1 anti-vinculin mouse antibody, goat anti-mouse IgG1 Alexa 555 antibody, atto-488-conjugated Phalloidin and Hoechst were purchased from Sigma Aldrich. Water was deionized prior to use using a Milli-Q Advantage A-10 equipped with a Q-Guard

 

T2 purification pack. Bovine serum albumin, γ-globulin from bovine blood and fibrinogen from bovine plasma were obtained from Sigma Aldrich as powders and used without further purification.

### Synthesis of mono-functional-PEG-BCN (3)

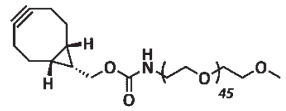

(3)

Methoxy poly(ethylene glycol) amine (359.0 mg, 0.343 mmol) and (1*R*,8*S*,9s)-bicyclo[6.1.0]non-4-yn-9-ylmethyl *N*-succinimidyl carbonate (76.6 mg) were dissolved in 3 mL dimethylformamide (DMF). 20 equivalents of di-isopropylethylamine (DIPEA) (597 μL, 3.43 mmol) were added and the reaction was stirred overnight under an argon atmosphere at room temperature. The reaction mixture was purified using a 2 kDa dialysis membrane in 4 L of Milli-Q water and stirred for 24 h. Water was changed 3 times in total. The reaction mixture was freeze-dried in the lyophilizer for 72 h, resulting in a white powder **3** (284.2 mg, 0.127 mmol, 79%). The product formation was confirmed by $^1$H-NMR and MALDI-ToF analysis (ESI Fig. S7†).

$^1$H-NMR (400 MHz, $CDCl_3$): $\delta$ 4.25–4.05 (d, 2H), 3.86–3.45 (m, 184H), 3.42–3.38 (s, 3H), 3.38–3.29 (d, 2H), 2.37–2.11 (m, 4H), 1.26–1.05 (m, 2H), 1.03–0.88 (m, 2H).

### Synthesis of bi-functional-PEG-BCN (4)

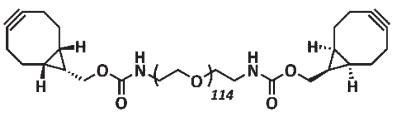

(4)

Poly(ethylene glycol)diamine (442.1 mg, 0.086 mmol) and (1*R*,8*S*,9s)-bicyclo[6.1.0]non-4-yn-9-ylmethyl *N*-succinimidyl carbonate (98.0 mg, 0.343 mmol) were dissolved in 3 mL dimethylformamide (DMF). 20 equivalents of di-isopropylethylamine (DIPEA) (299 μL, 1.72 mmol) were added and the reaction was stirred overnight under an argon atmosphere at room temperature. The reaction mixture was purified using a 2 kDa dialysis membrane in 4 L of Milli-Q water and stirred for 24 h. Water was changed 3 times in total. The reaction mixture was freeze-dried in the lyophilizer for 72 hours, resulting in a white powder **4** (389.2 mg, 0.072 mmol, 88%). The product formation was confirmed by $^1$H-NMR and MALDI-ToF analysis (ESI Fig. S8†).

$^1$H-NMR (400 MHz, $CDCl_3$): $\delta$ 4.25–4.08 (d, 4H), 3.87–3.44 (m, 456H), 3.43–3.32 (d, 4H), 2.76–2.66 (s, 2H), 2.38–2.15 (m, 8H), 1.25–1.07 (m, 4H), 1.07–0.83 (m, 4H).

### Synthesis of star-PEG-BCN (5)

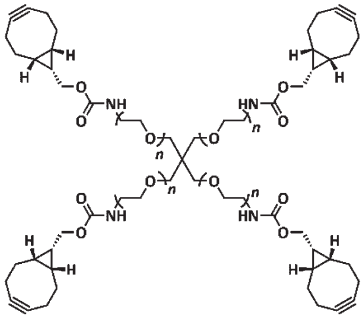

(5)

Four-arm poly(ethylene glycol)tetraamine ($M_n \sim 10\,000$ Da, $n \sim 57$, 1 g, 0.4 mmol $NH_2$, 1×, Jenkem) and BCN-OSu (175 mg, 0.015 mmol, 1.5×) were dissolved in dimethylformamide (5 mL). *N*,*N*-Diisopropylethylamine (277 μL, 207 mg, 1.6 mmol, 4×) was added to the mixture, and the reaction mixture was stirred overnight, concentrated, dissolved in water, dialyzed (molecular weight cutoff ~2 kDa, SpectraPor), and lyophilized to yield a white powder (1.06 g, quantitative yield).

$^1$H NMR (500 MHz, $CDCl_3$) $\delta$ 5.27 (s, 4H), 4.13 (d, $J$ = 8.0 Hz, 8H), 3.78–3.75 (m, 8H), 3.65–3.61 (m, 909H), 3.50–3.47 (m, 4H), 2.30–2.18 (m, 24H), 1.64–1.50 (m, 8H), 1.39–1.29 (m, 4H), 0.98–0.88 (m, 8H). Functionalization was confirmed to be >95% by $^1$H-NMR by comparing integral values for characteristic BCN peaks ($\delta$ 2.24, 1.57, 1.34, 0.92) with those from the PEG backbone ($\delta$ 3.63) (ESI Fig. S9†).

### Preparation of polymer solutions

Solutions of PCLdiUPy were prepared at a concentration of 20 mg mL$^{-1}$ in 1,1,1,3,3,3-hexafluoroisopropanol (HFIP). For the mixtures, 10 mol% UPy-Tz solutions were prepared by adding 10 mol% UPy-Tz to 90 mol% PCLdiUPy solutions. PEG solutions were prepared at different concentrations in ultrapure water, obtained using a Milli-Q Advantage A-10 equipped with a Q-Guard T2 purification pack.

### Preparation of spin coated surfaces

Spin coated samples were prepared by spin coating 50 μL of a solution of 20 mg mL$^{-1}$ PCLdiUPy or PCLdiUPy with 10 mol% UPy-Tz at 3000 rpm for 30 seconds on glass coverslips (∅ 12 mm, thickness 1 mm) or gold-coated sensors (BiolinScientific AB). Samples conjugated with a BCN functionalized PEG polymer were prepared by incubating spin coated samples with 0.5 or 0.1 mg mL$^{-1}$ PEG solution for 90 minutes at room temperature. The samples were washed for 10 minutes in Milli-Q water and dried with air before continuing experiments.

### Atomic force microscopy

Atomic force microscopy was performed at room temperature on spin-coated films using a Digital Instrument Multimode Nanoscope IV 279 with silicon cantilever tips (PPP-NCH-50, 204–497 kHz, 10–130 N m$^{-1}$ from Nanosensors) using a tapping regime mode. The roughness of the surface has been

measured and images have been processed using Gwyddion software (version 2.39).

### X-ray photoelectron spectroscopy

X-ray photoelectron spectroscopy was performed on spin-coated coverslips and were recorded using a Thermo Scientific K-alpha spectrometer equipped with a monochromatic, small-spot X261 ray source and a 180° double focusing hemispherical analyzer with a 128-channel detector. The coverslips were mounted on the holder using a carbon tape and an aluminum anode (Al Kα, 1486.6 eV, 72 W) was used to obtain the spectra. Analysis and quantification of the spectra were performed using CasaXPS software version 2.3.16, using the C 1s, N 1s, O 1s and F 1s regions.

### Water contact angle measurements

Water contact angles were measured on spin-coated surfaces at room temperature in air using an OCA 30 (DataPhysics). Deionized water droplets of 4 μL were applied on the surface of the spin-coated coverslips and coverslips conjugated to the BCN functionalized PEG polymers. Images were recorded at a rate of 2.5 frames per second and the angle at the polymer–air–water interface was measured after 5 seconds using an automatic fitting routine (SCA20 software).

### Quartz-crystal microbalance with dissipation monitoring

QCM-D measurements were performed on the Q-Sense E4 instrument (BiolinScientific) using gold-coated AT-cut quartz discs with a fundamental frequency of 4.95 MHz (QSX 301 Gold, BiolinScientific AB). Before use, sensors were rinsed with piranha solution and subsequently heated for 15 minutes at 70 °C in a 4 : 1 : 1 mixture of ultrapure water, ammonia and 30% hydrogen peroxide (base piranha). Subsequently, sensors were rinsed with water and acetone and dried with nitrogen gas. Clean crystals were mounted to record their fundamental frequency in air and subsequently removed for spin coating.

All experiments were performed at 20 °C. After equilibration, the frequency and dissipation of the sensors were measured in air for 1 minute. After mounting the sensors with the spin-coated material, sensors were again measured in air for 1 minute. The frequency and dissipation changes of the sensor before spin-coating and after spin-coating were stitched and Sauerbrey was applied to the stitched data to determine the layer thickness. After mounting the PEG-BCN to the sensor surfaces, PBS was passed over the surface at 0.1 mL $min^{-1}$ until the signal equilibrated. Subsequently, the protein solution was passed over the surface at 0.1 mL $min^{-1}$ (I). Frequency and dissipation changes were recorded for 30 minutes, and the sensors were rinsed with PBS (II). Each experiment was repeated in twice, and means and standard errors of the mean are reported.

After each experiment, the system was cleaned by rinsing with PBS for 10 minutes, followed by 50 mL of a 2 wt% solution of Hellmanex III (Hellma) in ultrapure water, followed by rinsing with ultrapure water for 10 minutes. Next, the sensors were removed and the components were dried using nitrogen.

### Visco-elastic modeling of the data

Shifts in frequency and dissipation for overtones 3, 5, 7, 9 and 11 were analyzed using the Voigt–Voinova model and the QTools software (Q-sense). As is evident from the measurements, the viscosity of the protein solutions was higher than the viscosity of PBS. Therefore, the viscosity of the protein solution was accounted in the model by the use of a 1 layer (L1) viscoelastic model with a viscosity of 0.001 Pa s and a fluid density of 1100 kg $m^{-3}$. The protein layer density was set to 1145 kg $m^{-3}$ for all protein layers as found in the literature. The minimum and maximum estimate for the fitted parameters of L1 viscosity, L1 shear and L1 thickness were set between 0.0001–0.1, 1000–$1\times10^{-8}$ and $1\times10^{-11}$–$1\times10^{-7}$, respectively. A 2nd order polynomial model was used to estimate the standard deviation. The data were fitted by using a descending incremental fitting mode with a first row to fit the grid mode. The model was optimized by decreasing $\chi^2$ by tuning the selection of overtones.

### HK-2 cell culture

Human proximal tubule epithelial kidney-2 (HK-2) cells were obtained from ATCC; immortalized proximal tubule epithelial cells were thawed from a liquid $N_2$ tank and cultured in a 0.1% gelatin/PBS pre-coated T75 flask in a complete medium. The complete medium consisted of DMEM with 10 vol% FBS and 1 vol% penicillin–streptomycin solutions. Cells were cultured up to 80–90% confluence at 37 °C and 5% $CO_2$ in a humidified atmosphere. Cells were washed with PBS twice and 0.05% trypsin–EDTA was used 2–3 minutes to detach the cells from the culture flask. Trypsin was inactivated by the addition of the complete medium and cell suspension was transferred to a 15 mL falcon tube and centrifuged at 1000 rpm for 5 minutes. The supernatant was aspirated and the cell pellet was re-suspended in the complete medium. Cell concentrations were determined *via* cell counting by the use of a hemocytometer.

### HK-2 cell seeding on spin-coated scaffolds

Transwell inserts were sterilized in a 70% ethanol bath and placed in a LAF-cabinet to evaporate the ethanol from the inserts. Spin-coated coverslips were placed in the bottom ring of the transwells using sterile forceps. The top of the insert was placed on top of the bottom ring and transferred to a 12-well plate. The coverslips were sterilized under UV for 30 minutes.

Cells were trypsinized and cell concentration was determined *via* cell counting in a hemocytometer. The cells were diluted until a concentration of 60 000 cells per mL and 500 μL of cell suspension was added to each transwell insert. The cells were cultured for 24 h, 72 h or one week at 37 °C and 5% $CO_2$ in a humidified atmosphere. The cell medium was changed once for the 72 h culture and twice for the 1-week culture.

### HK-2 cell culture procedure in competition assay

Transwell inserts were sterilized in 70% ethanol bath and placed in a LAF-cabinet to evaporate the ethanol from the

 

inserts. Spin-coated coverslips were placed in the bottom ring of the transwells using sterile forceps. The top of the insert was placed on top of the bottom ring and transferred to a 12-well plate. The coverslips were sterilized under UV for 30 minutes.

PEG-BCN powder was diluted in the complete medium until a concentration of 0.5 mg $mL^{-1}$. Cells were trypsinized and cell concentration was determined *via* cell counting in a hemocytometer. The cells were diluted until a concentration of 60 000 cells per mL. The cells were divided in four 15 mL falcon tubes and centrifuged at 1000 rpm for 5 minutes. The supernatant was aspirated and the cell pellet was resuspended in PEG-BCN solutions in the complete medium. 500 μL of cell suspension was added to each transwell insert and cells were cultured for 24 h or 72 h at 37 °C and 5% $CO_2$ in a humidified atmosphere. The cell medium was changed once for the 72 h culture.

### HK-2 cell fixation, staining and visualization

After the culture period, scaffolds were washed three times with PBS. Cells were fixed in 3.7% formaldehyde in PBS and permeabilized in 0.5% Triton-X 100 buffer for 20 minutes. Coverslips were washed three times with PBS and blocked in 500 μL 5 wt/vol% BSA solution in PBS for 45 minutes. Coverslips were removed from the transwell inserts and placed cell-side up on a parafilm covered glass plate in a moisturized chamber. Anti-vinculin (monoclonal IgG1 anti-vinculin mouse antibody) was diluted in a 2% BSA in PBS solution at a concentration of 1 : 400 and 50 μL of solution was incubated at room temperature for 90 minutes. Cells were washed twice with PBS before incubation with a goat anti-mouse IgG1 Alexa 555 antibody (1 : 200) diluted in 2% BSA in PBS solution with Phalloidin Atto 488 (1 : 1000) for 60 minutes at room temperature. Then, cell nuclei were stained with Hoechst (1 : 1000) for 15 minutes at room temperature. The coverslips were washed five times with PBS and mounted on microscope slides using a Mowiol. The samples were visualized by fluorescence microscopy using a 10× and 20× magnifying objective on a Zeiss Axio observer D1 equipped with an AxioCam Mrm camera and Zeiss Axiovision software (Carl Zeiss).

## Conclusions

In a modular fashion, UPy-modified tetrazine additives were incorporated into a supramolecular UPy-polymer. *Via* an inverse Diels–Alder cycloaddition between the UPy-Tz and a BCN-modified PEG-polymer, the surface of the material was selectively functionalized, thereby creating a completely anti-fouling material surface. Moreover, it was shown that the extent of anti-fouling behavior is strongly dependent on the type of PEG-BCN polymer that was reacted, *i.e.* a mono-functional-PEG-BCN displayed less efficient anti-fouling properties as compared to bi-functional-PEG-BCN and the best performing star-PEG-BCN. The star-PEG-BCN showed excellent resistance to both protein adsorption and cell adhesion, which is attributed to the architecture of the polymer that is able to react up to four times at the material surface.

These results hold great promise in the development of functional supramolecular biomaterials that exhibit selective surface functionality. The introduction of anti-fouling coatings at surfaces has been widely investigated in the literature,[30,48–54] however examples where the covalent attachment of such coatings at supramolecular surfaces is investigated are scarce. Upon the introduction of the anti-fouling coating, the materials are prevented from nonspecific protein and cell adhesion. Next steps involve the selective introduction of bioactive cues, which enables the modification of the materials with the desired bioactive functionality towards specific regenerative medicine applications.

## Acknowledgements

We thank E. W. Meijer for critical reading of the manuscript and useful discussions on the results, H. M. Janssen and H. M. Keizer from SyMO-Chem BV, Eindhoven, The Netherlands, for useful discussions and synthesis of the UPy-Tz additive, M. O. Grillaud for useful discussions and help with synthesis, M. W. G. M. Verhoeven for XPS collaboration and the ICMS Animation Studio for careful design of cartoons. This work was financially supported by the European Research Council (FP7/2007–2013) ERC Grant Agreement 308045 and the Ministry of Education, Culture and Science (Gravity program 024.001.03).

## Notes and references

1 P. Thevenot, W. Hu and L. Tang, *Curr. Top. Med. Chem.*, 2008, **8**, 270–280.
2 C. Chen, S. Bang, Y. Cho, S. Lee, I. Lee, S. Zhang and I. Noh, *Biomater. Res.*, 2016, **20**, 10.
3 V. B. Damodaran and N. S. Murthy, *Biomater. Res.*, 2016, **20**, 18.
4 D. W. Grainger, *Nat. Biotechnol.*, 2013, **31**, 507–509.
5 Q. Wei, T. Becherer, S. Angioletti-Uberti, J. Dzubiella, C. Wischke, A. T. Neffe, A. Lendlein, M. Ballauff and R. Haag, *Angew. Chem., Int. Ed.*, 2014, **53**, 8004–8031.
6 E. F. Leonard and L. Vroman, *J. Biomater. Sci., Polym. Ed.*, 1991, **3**, 95–107.
7 J. E. Gittens, T. J. Smith, R. Suleiman and R. Akid, *Biotechnol. Adv.*, 2013, **31**, 1738–1753.
8 I. Banerjee, R. C. Pangule and R. S. Kane, *Adv. Mater.*, 2011, **23**, 690–718.
9 S. Chen, L. Li, C. Zhao and J. Zheng, *Polymer*, 2010, **51**, 5283–5293.
10 S. I. Jeon, J. H. Lee, J. D. Andrade and P. G. De Gennes, *J. Colloid Interface Sci.*, 1991, **142**, 149–158.
11 F. Fuertges and A. Abuchowski, *J. Controlled Release*, 1990, **11**, 139–148.

12 K. L. Prime and G. M. Whitesides, *J. Am. Chem. Soc.*, 1993, **115**, 10714–10721.
13 P. K. Thalla, A. A. Contreras-Garcia, H. Fadlallah, J. Barrette, G. De Crescenzo, Y. Merhi and S. Lerouge, *BioMed Res. Int.*, 2013, **2013**, e962376.
14 C. Strehmel, H. Perez-Hernandez, Z. Zhang, A. Löbus, A. F. Lasagni and M. C. Lensen, *ACS Biomater. Sci. Eng.*, 2015, **1**, 747–752.
15 E. Ostuni, R. G. Chapman, M. N. Liang, G. Meluleni, G. Pier, D. E. Ingber and G. M. Whitesides, *Langmuir*, 2001, **17**, 6336–6343.
16 Z. Zhang, J. Wang, Q. Tu, N. Nie, J. Sha, W. Liu, R. Liu, Y. Zhang and J. Wang, *Colloids Surf., B*, 2011, **88**, 85–92.
17 W. J. Yang, K.-G. Neoh, E.-T. Kang, S. L.-M. Teo and D. Rittschof, *Prog. Polym. Sci.*, 2014, **39**, 1017–1042.
18 J. Wang and J. Li, *Mater. Lett.*, 2017, **186**, 178–181.
19 L.-L. Li, G.-B. Qi, F. Yu, S.-J. Liu and H. Wang, *Adv. Mater.*, 2015, **27**, 3181–3188.
20 P. Liu, T. Huang, P. Liu, S. Shi, Q. Chen, L. Li and J. Shen, *J. Colloid Interface Sci.*, 2016, **480**, 91–101.
21 W. J. Yang, D. Pranantyo, K.-G. Neoh, E.-T. Kang, S. L.-M. Teo and D. Rittschof, *Biomacromolecules*, 2012, **13**, 2769–2780.
22 A. M. Laradji, C. D. McNitt, N. S. Yadavalli, V. V. Popik and S. Minko, *Macromolecules*, 2016, **49**, 7625–7631.
23 P. Hu, T. Jiang, H. Ni, P. Ye, Z. Han, Z. Zhao, C. Zhu and X. Lu, *Polym. Bull.*, 2016, **73**, 1405–1426.
24 Z. X. Voo, M. Khan, K. Narayanan, D. Seah, J. L. Hedrick and Y. Y. Yang, *Macromolecules*, 2015, **48**, 1055–1064.
25 K. Chen, S. Zhou and L. Wu, *RSC Adv.*, 2015, **5**, 104907–104914.
26 J. Deng, X. Liu, S. Zhang, C. Cheng, C. Nie and C. Zhao, *Langmuir*, 2015, **31**, 9665–9674.
27 H. Shi, H. Liu, S. Luan, D. Shi, S. Yan, C. Liu, R. K. Y. Li and J. Yin, *Compos. Sci. Technol.*, 2016, **127**, 28–35.
28 Y. Chen, X. Zhao and C. He, *RSC Adv.*, 2015, **5**, 68998–69005.
29 Y. Dang, M. Quan, C.-M. Xing, Y.-B. Wang and Y.-K. Gong, *J. Mater. Chem. B*, 2015, **3**, 2350–2361.
30 J. L. Dalsin, B.-H. Hu, B. P. Lee and P. B. Messersmith, *J. Am. Chem. Soc.*, 2003, **125**, 4253–4258.
31 L. Qun Xu, D. Pranantyo, K.-G. Neoh, E.-T. Kang, S. Lay-Ming Teo and G. Dong Fu, *Polym. Chem.*, 2016, **7**, 493–501.
32 R. P. Sijbesma, F. H. Beijer, L. Brunsveld, B. J. Folmer, J. H. Hirschberg, R. F. Lange, J. K. Lowe and E. W. Meijer, *Science*, 1997, **278**, 1601–1604.
33 B. J. B. Folmer, R. P. Sijbesma, R. M. Versteegen, J. a. J. van der Rijt and E. W. Meijer, *Adv. Mater.*, 2000, **12**, 874–878.
34 P. Y. W. Dankers, M. C. Harmsen, L. A. Brouwer, M. J. A. Van Luyn and E. W. Meijer, *Nat. Mater.*, 2005, **4**, 568–574.
35 D. E. P. Muylaert, G. C. van Almen, H. Talacua, J. O. Fledderus, J. Kluin, S. I. S. Hendrikse, J. L. J. van Dongen, E. Sijbesma, A. W. Bosman, T. Mes, S. H. Thakkar, A. I. P. M. Smits, C. V. C. Bouten, P. Y. W. Dankers and M. C. Verhaar, *Biomaterials*, 2016, **76**, 187–195.
36 G. C. van Almen, H. Talacua, B. D. Ippel, B. B. Mollet, M. Ramaekers, M. Simonet, A. I. P. M. Smits, C. V. C. Bouten, J. Kluin and P. Y. W. Dankers, *Macromol. Biosci.*, 2016, **16**, 350–362.
37 A. C. H. Pape, B. D. Ippel and P. Y. W. Dankers, *Langmuir*, 2017, **33**(16), 4075–4082.
38 B. B. Mollet, M. Comellas-Aragonès, A. J. H. Spiering, S. H. M. Söntjens, E. W. Meijer and P. Y. W. Dankers, *J. Mater. Chem. B*, 2014, **2**, 2483–2493.
39 O. J. G. M. Goor, H. M. Keizer, A. L. Bruinen, M. G. J. Schmitz, R. M. Versteegen, H. M. Janssen, R. M. A. Heeren and P. Y. W. Dankers, *Adv. Mater.*, 2017, **29**, 1604652.
40 M. L. Blackman, M. Royzen and J. M. Fox, *J. Am. Chem. Soc.*, 2008, **130**, 13518–13519.
41 C. S. McKay and M. G. Finn, *Chem. Biol.*, 2014, **21**, 1075–1101.
42 G. Morgese, L. Trachsel, M. Romio, M. Divandari, S. N. Ramakrishna and E. M. Benetti, *Angew. Chem., Int. Ed.*, 2016, **55**, 15583–15588.
43 M. Tagaya, *Polym. J.*, 2015, **47**, 599–608.
44 X. Wang, X. Hu, I. Dulińska-Molak, N. Kawazoe, Y. Yang and G. Chen, *Sci. Rep.*, 2016, **6**, 28708.
45 R. Rossin, P. R. Verkerk, S. M. van den Bosch, R. C. M. Vulders, I. Verel, J. Lub and M. S. Robillard, *Angew. Chem., Int. Ed.*, 2010, **49**, 3375–3378.
46 N. K. Devaraj, S. Hilderbrand, R. Upadhyay, R. Mazitschek and R. Weissleder, *Angew. Chem., Int. Ed.*, 2010, **49**, 2869–2872.
47 K. Lang, L. Davis, J. Torres-Kolbus, C. Chou, A. Deiters and J. W. Chin, *Nat. Chem.*, 2012, **4**, 298–304.
48 B. S. Flavel, M. Jasieniak, L. Velleman, S. Ciampi, E. Luais, J. R. Peterson, H. J. Griesser, J. G. Shapter and J. J. Gooding, *Langmuir*, 2013, **29**, 8355–8362.
49 C. Wang, C. Ma, C. Mu and W. Lin, *Langmuir*, 2014, **30**, 12860–12867.
50 N. Y. Kostina, O. Pop-Georgievski, M. Bachmann, N. Neykova, M. Bruns, J. Michálek, M. Bastmeyer and C. Rodriguez-Emmenegger, *Macromol. Biosci.*, 2016, **16**, 83–94.
51 L. Q. Xu, D. Pranantyo, K.-G. Neoh, E.-T. Kang, S. L.-M. Teo and G. D. Fu, *Colloids Surf., B*, 2016, **141**, 65–73.
52 H. P. Felgueiras, L. M. Wang, K. F. Ren, M. M. Querido, Q. Jin, M. A. Barbosa, J. Ji and M. C. L. Martins, *ACS Appl. Mater. Interfaces*, 2017, **9**, 7979–7989.
53 N. Hui, X. Sun, S. Niu and X. Luo, *ACS Appl. Mater. Interfaces*, 2017, **9**, 2914–2923.
54 Z. Zhi, Y. Su, Y. Xi, L. Tian, M. Xu, Q. Wang, S. Padidan, P. Li and W. Huang, *ACS Appl. Mater. Interfaces*, 2017, **9**, 10383–10397.

 